Electrical resistivity imaging of the architecture of substream sediments

N. Crook,[1] A. Binley,[2] R. Knight,[1] D. A. Robinson,[1,3] J. Zarnetske,[4] and R. Haggerty[4]

Received 1 March 2008; revised 12 August 2008; accepted 3 September 2008; published 9 December 2008.

[1] The modeling of fluvial systems is constrained by a lack of spatial information about the continuity and structure of streambed sediments. There are few methods for noninvasive characterization of streambeds. Invasive methods using wells and cores fail to provide detailed spatial information on the prevailing architecture and its continuity. Geophysical techniques play a pivotal role in providing spatial information on subsurface properties and processes across many other environments, and we have applied the use of one of those techniques to streambeds. We demonstrate, through two examples, how electrical resistivity imaging can be utilized for characterization of subchannel architecture. In the first example, electrodes installed in riparian boreholes and on the streambed are used for imaging, under the river bed, the thickness and continuity of a highly permeable alluvial gravel layer overlying chalk. In the second example, electrical resistivity images, determined from data collected using electrodes installed on the river bed, provide a constrained estimate of the sediment volume behind a log jam, vital to modeling biogeochemical exchange, which had eluded measurement using conventional drilling methods owing to the boulder content of the stream. The two examples show that noninvasive electrical resistivity imaging is possible in complex stream environments and provides valuable information about the subsurface architecture beneath the stream channels.

Citation: Crook, N., A. Binley, R. Knight, D. A. Robinson, J. Zarnetske, and R. Haggerty (2008), Electrical resistivity imaging of the architecture of substream sediments, *Water Resour. Res.*, *44*, W00D13, doi:10.1029/2008WR006968.

1. Introduction

[2] One of the challenges in studying rivers and streams is quantification of the subsurface properties. At most sites, information about subsurface properties and processes has been obtained using wells or trenches. Wells and trenches are spatially limited and often cannot be installed more than a meter or two because site access prevents the use of large drilling/coring equipment [e.g., *Wondzell*, 2006; *Burkholder et al.*, 2008]. Given the pervasive spatial and temporal heterogeneity of the subsurface, however, such localized measurements cannot provide the density of sampling (spatial or temporal) required to accurately characterize subsurface properties and processes. In order to address the need for improved forms of subsurface measurement, geophysical techniques are increasingly applied to noninvasively sample or ''image'' subsurface regions. These geophysical techniques can provide a means of obtaining information about the subsurface that cannot be acquired through other, existing forms of measurement.

[3] One of the critical elements in many hydrologic systems is the dynamic exchange between surface water and groundwater along the bed of rivers and streams, in the hyporheic zone. The movements of water within the hyporheic zone are key regulators of head and nutrients in many riverine ecosystems [*Jones and Mulholland*, 1999]. Studies of the processes operating in this zone currently rely on the direct sampling of the surface water chemistry, installation of shallow wells, use of natural and artificial tracers, and testing of hydraulic properties, either in situ or from core samples. What cannot be readily obtained from these measurements is an accurate ''image'' of the large-scale architecture of the streambed materials through which the surface water-groundwater exchange takes place. Combining geophysical investigations with the traditional methods highlighted can provide better informed subsurface characterizations together with information on subsurface processes. We demonstrate, in examples from the United Kingdom and the United States, the usefulness of the geophysical technique referred to as electrical resistivity imaging (sometimes also referred to as electrical resistivity tomography) to obtain high-resolution images of these underlying materials. This application of geophysical imaging provides an important new approach to characterize a critical region at the interface between surface water and groundwater.

[4] Electrical resistivity imaging (ERI) uses electrodes located on the surface or in boreholes/wells to obtain an image of the electrical properties of a subsurface region. In ERI, current is injected between two electrodes and potential measurements are made at a number of other electrode

[1]Department of Geophysics, Stanford University, Stanford, California, USA.
[2]Lancaster Environment Centre, Lancaster University, Lancaster, UK.
[3]Now at Department of Food Production, University of West Indies, St. Augustine, Trinidad and Tobago.
[4]Department of Geosciences, Oregon State University, Corvallis, Oregon, USA.

Copyright 2008 by the American Geophysical Union.
0043-1397/08/2008WR006968

pairs. This is repeated many times using multiple combinations of tens or hundreds of electrode pairs. These data are inverted to determine a model that best represents the subsurface electrical resistivity structure. A more detailed explanation of ERI theory and methodology can be found in the work of *Binley and Kemna* [2005]. For our modeling in the examples here we use a triangular finite element-based forward solution coupled with an ''Occam's'' style inversion [e.g., *Constable et al.*, 1987]. The use of an ''Occam's'' style inversion produces a smooth model that fits a data set within certain tolerances. The model allows specification of electrode locations at any node within the finite element mesh. Thus, as is the case in the following examples, the effect of conductive features such as a water column covering a number of the electrode locations can be incorporated into the inversion.

[5] The final product, a 2-D or 3-D resistivity image, is interpreted using information about the link between the electrical resistivity and subsurface material properties. ERI has been used for a wide range of applications in hydrology, by taking advantage of the link between the estimated geophysical property, electrical resistivity, and material properties such as clay content, water content, and salinity. Hydrological examples include monitoring flow and transport in the vadose zone [e.g., *Daily et al.*, 1992; *al Hagrey and Michaelsen*, 1999]; tracking tracer migration in the saturated zone [e.g., *Kemna et al.*, 2002; *Singha and Gorelick*, 2005]; estimation of hydraulic properties [*Binley et al.*, 2002; *Singha et al.*, 2007].

[6] The objective of our research was to build on recent ERI advancements to demonstrate its use as a means of determining the geometry of sediment packages underlying streambeds. Imaging the subchannel sediment architecture presents a departure from the typical electrical resistivity surveys, in that the electrodes need to be submerged within the stream water column or physically embedded in the saturated streambed sediments. A recent advance in ERI equipment, for waterborne surveys, includes the use of streamer resistivity techniques. Typically this involves towing an array of electrodes after a vessel, suspended in the water column using a series of floats. With the available resistivity systems, the first two electrodes are used as the current dipole, with the remaining electrodes making up the receiver dipoles (current technology allows for between 2 and, typically, 10 receiver dipoles). Electrical measurements are taken continuously together with GPS and sonar measurements, for the electrode positions and water depth respectively. Applications of this ERI streamer technology include mapping submarine groundwater discharge in estuarine environments [*Day-Lewis et al.*, 2006; *Breier et al.*, 2005; *Manheim et al.*, 2004]; monitoring the discharge of nitrate-containing groundwater into the marine environment [*Andersen et al.*, 2007]; and delineation of faults beneath riverbeds [*Kwon et al.*, 2005].

[7] In some cases, electrodes may be deployed in boreholes, thus allowing higher-resolution of subsurface structures at depth. This approach has been demonstrated in groundwater studies [e.g., *Slater et al.*, 1997; *Kemna et al.*, 2004]. *Acworth and Dasey* [2003] have also shown potential use of such deployment for groundwater-surface water interaction studies.

[8] Another deployment technique, which has received little attention in the literature, is the emplacement of the electrodes directly in the streambed. In many watersheds the above streamer technique would be unfeasible owing to channel tortuosity, inadequate water column thickness, and complex channel geomorphology. Thus in small headwater or upland watersheds where the water column depth, channel structure or energy of environment is highly variable (e.g., riffle or step-pool features, braided river systems, barriers, and topographical steps) the direct emplacement of electrodes in the streambed becomes a feasible option.

[9] Figure 1 illustrates, from a synthetic model study, how deployment of electrodes on a streambed can enhance significantly the resolution of the subsurface. The resistivity model in Figure 1a represents a vertical longitudinal cross section along a short reach. The stream water resistivity of 100 Ωm is equivalent to an electrical conductivity of 100 μScm^{-1}. The water column thickness varies between 0.4 and 0.8 m along the model reach. Beneath the stream a high-resistivity (representing low porosity) unit (of 2000 Ωm) that varies in thickness overlies a uniform aquifer bedrock of 500 Ωm. A forward model of measurements made in a dipole-dipole configuration (see *Binley and Kemna* [2005] for an explanation) on an array of 48 electrodes at 0.5-m intervals was computed for the case with electrodes deployed on a conventional surface streamer array and with electrodes placed on the streambed. Figures 1b and 1c show the inversion results for these two cases. A comparison of the two results reveals the significant deterioration of vertical resolution for the conventional streamer array case, even for such a shallow stream. Note that the poor recovery of the target structure at each end of the image (as always seen in surface ERI images) is a result of reduced sensitivity owing to poor electrode coverage. Although not considered here, it may be possible to enhance resistivity images in applications such as this by allowing regions within the inverse model to be ''disconnected,'' as illustrated by *Slater and Binley* [2006] in their study of permeable reactive barriers. Such boundaries may exist in the present study, e.g., at the known stream-streambed interface.

[10] Here we present two examples of field studies designed to investigate and develop the use of ERI for mapping the sediment architecture underlying and/or within streambeds. The first example is the use of ERI to delineate the lateral, spatial extent of alluvial sediments in an English lowland river. This study forms part of the UK Natural Environment Research Council's (NERC) Lowland Catchment Research (LOCAR) program. The second example demonstrates the use of ERI to map the distribution (longitudinal extent and thickness) of sediment overlying bedrock, trapped behind a debris jam in the H. J. Andrews Experimental Forest, Oregon, USA. These two field studies represent a significant advance, compared to traditional hydrogeological methods, in our ability to noninvasively image the extent and architecture of substream sediments.

2. River Lambourn, Berkshire, UK

2.1. Site Description and Motivation

[11] The River Lambourn is located within the West Berkshire Downs, UK (Figure 2a). The catchment of the River Lambourn extends over 234 km^2, with elevation

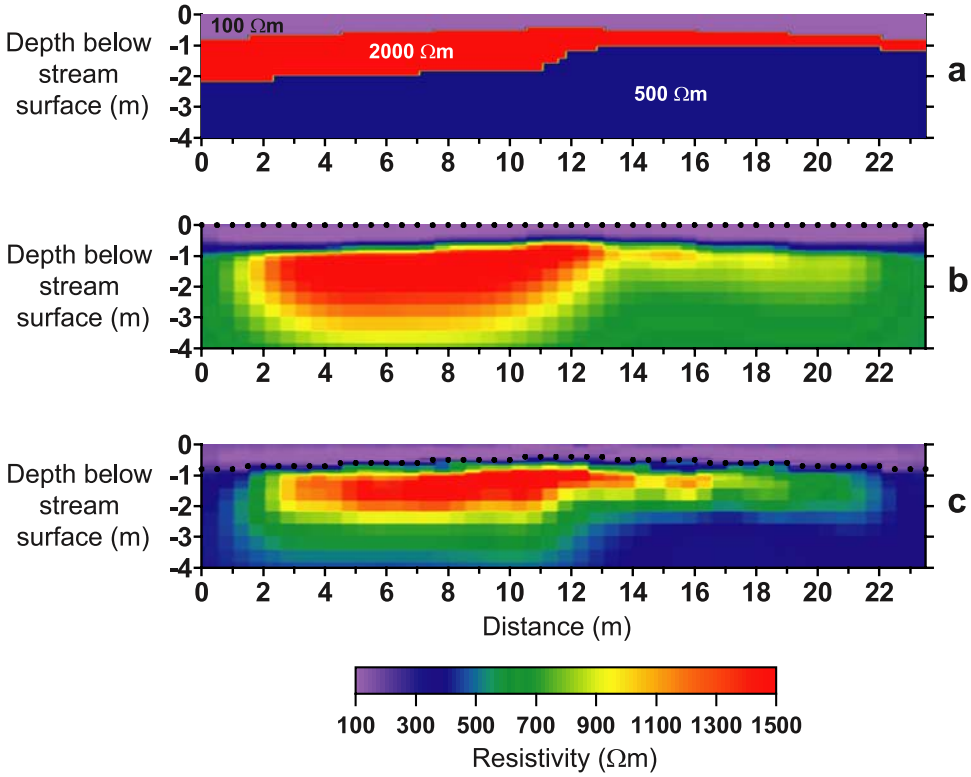

Figure 1. Synthetic model results showing effect of stream on resolution of resistivity. (a) Synthetic three-layer model (top layer represents stream). (b) Inversion of resistivity data from survey with electrodes located on stream surface. (c) Inversion of resistivity data with electrodes located on streambed.

ranging from 261 m in the northwest to around 70 m in the southeast [*Grapes et al.*, 2005]. The river is fed by the Chalk aquifer. In the valley bottom floodplain region, overlying the Chalk aquifer, is an alluvial gravel aquifer. This alluvial gravel aquifer is discontinuous along the length of the stream channel, with a thickness that varies considerably, dependent in part on the size of the associated floodplain.

[12] The Chalk is the most important aquifer within the UK, extending over an area of ~21500 km^2 and providing approximately 53% of the country's groundwater [*Bradford*, 2002]. Of concern is the fact that groundwater-fed rivers associated with the Chalk aquifer are under increasing threat from groundwater extraction, flood relief measures, changes in river management and agricultural practice, and from sources of point and nonpoint source pollution [*Grapes et al.*, 2005]. For example, the Chalk aquifer is potentially a long-term source of river nitrates [*Bradford*, 2002], which in turn directly effects the aquatic and riparian ecosystem nutrient dynamics.

[13] A thorough understanding of the mechanisms by which stream-groundwater interactions occur is required for the effective management of both surface water and groundwater resources [*Grapes et al.*, 2006]. At present, the representation of stream-groundwater interactions tends to be highly generalized, typically produced by regional-scale models on the catchment scale. A recent review of stream-groundwater interactions highlighted the need for improved characterization of interfaces, such as between a bedrock and alluvial aquifer, in order to accurately model the interactions at a range of temporal and spatial scales [*Sophocleous*, 2002]. Within the Lambourn catchment, *Grapes et al.* [2006] have demonstrated the importance of the alluvial gravel aquifer to maintaining stable water levels in floodplain wetland. Models of groundwater flow within the catchment require reliable delineation of hydrogeological units. Currently, the lack of accurate descriptions of the variability in spatial coverage and thickness of the alluvial gravel aquifer geometry is a major limiting factor in the understanding of the associated complex groundwater flow pathways and interactions. The use of ERI or other shallow subsurface geophysical techniques, therefore, presents an opportunity to constrain these limitations and advance our understanding of the Lambourn catchment aquifers.

[14] Typically, information on aquifers is obtained from borehole and well geological logs, the spatial distribution of such 1-D profiles can be highly variable, leading to large uncertainties in variations and continuity of subsurface structure. This inevitably leads to errors and uncertainty within conceptual models which can often diminish the usefulness of the resulting simulations. When combined with ground-truthing, geophysical techniques can provide the spatial coverage and resolution required to accurately image the subsurface of study areas. For the remainder of this section, we present the findings of one field experiment designed to determine the thickness and continuity of the alluvial aquifer below the River Lambourn using the ERI technique.

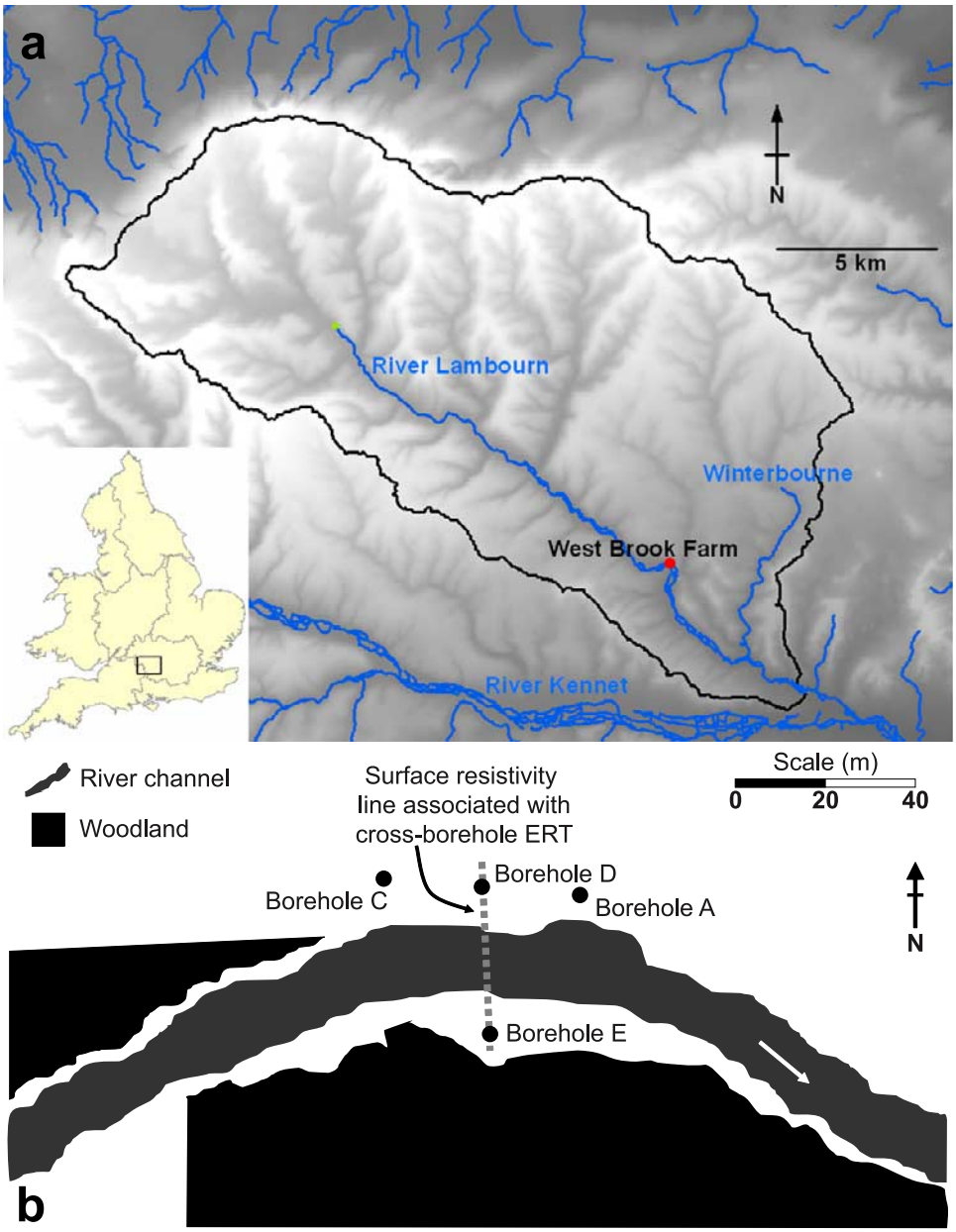

Figure 2. (a) Map of the Lambourn catchment within West Berkshire, UK (as noted on the inset map), and the location of the Lambourn River, West Brook Farm site. (b) Plan view schematic of the West Brook Farm site showing the location of the boreholes and surface electrode line relative to the Lambourn River.

2.2. Methodology

[15] As part of the LOCAR infrastructure development a number of monitoring borehole clusters were installed within the Lambourn catchment. The West Brook Farm site (Figure 2b) was instrumented with 9 observations boreholes (only the 4 boreholes closest to the stream channel are shown in Figure 2b) in a transect extending across the floodplain on both sides of the stream channel and extending up the hillslope to the north. During completion of the 4 floodplain boreholes closest to the stream channel, electrode arrays were installed for electrical resistivity surveys. These borehole arrays consisted of 50 electrodes constructed from cylindrical sections of stainless steel mesh (50 mm long by 25 mm in diameter) attached to one of the nested PVC piezometers at 0.5-m intervals.

[16] ERI was carried out between boreholes D and E at the West Brook Farm site in March 2005 (Figure 2b). These boreholes are located on either side of the stream, each approximately 5 m from the edge of the stream channel. The pole-pole electrode configuration (for details on the electrode configuration see *Binley and Kemna* [2005]) was used in this survey: the remote electrodes were placed on opposite sides of the stream, each more than 200-m distance from the stream channel (>5 times the maximum electrode separation). A combination of 32 surface electrodes (at 1-m spacing), 64 borehole electrodes (at 0.5-m spacing, with 32 in each borehole) and 2 remote electrodes was used; this

produced a total of 6022 four electrode resistance measurements. The surface electrodes were placed at 1-m intervals along a transect running between the two boreholes across the stream channel (with a 0.5-m interval between borehole and 2 closest electrodes in both cases).

[17] Those electrodes located within the streambed sediments were electrically insulated from the water column to reduce current leakage direct to the stream channel. The traditional multicore cables used for surface imaging surveys are not designed to be submerged, so the multicore cables were suspended beneath a supporting line installed across the stream channel using Velcro ties. An insulated extension wire was connected between the electrode and the suspended multicore cable. Typical 0.3-m-long stainless steel electrodes were modified for deployment within the stream. The connecting wire was attached to a hole drilled in the electrode, the top 0.1 m of which was sealed using a plastic covering glued in place. The bottom ~0.2 m of the electrodes were installed in the stream channel sediments, leaving the exposed ~0.1 m insulated from the water column by the plastic covering. All electrode locations were surveyed using a total station, and the depth of the water column was measured for those electrodes installed in the streambed for inclusion into the data inversion process.

[18] Resistance measurements were made using a 64 channel Campus Tomoplex meter. To make the most efficient use of the 64 available channels, data were collected using the 32 surface electrodes in combination with: first the top 16 electrodes in each borehole and then for the bottom 16 electrodes in each borehole. The results were then combined into a single file for inversion.

[19] Measurements of resistance inevitably contain errors owing to a variety of sources, including poor electrode contact, random device errors and external effects. An accurate assessment of these errors is critical to the efficiency of the inversion process. *Binley et al.* [1995] have shown that a good estimate of data error is achieved by considering the reciprocal error: the switching of current and potential electrodes should provide the transfer resistance value and any deviation from this provides an error quantification. This method of error quantification was adopted for this study. The reciprocal errors were found to be <10% for the survey and measurements with reciprocal errors >5% were omitted from the cross-borehole inversion. Assessment of the reciprocal errors in the data acquisition stage show that approximately 75% of the original 6022 readings collected displayed errors below the 5% cutoff. The majority of the reciprocal errors above 5% can be attributed to a number of the borehole electrodes being damaged in the installation phase leading to intermittent errors and poor electrical contact with the surrounding material. The relatively high cutoff used in this study can also be attributed to the effects of the damaged electrodes mentioned above. Note that in some applications of cross-borehole electrical resistivity a much lower rejection threshold is possible: errors will often be influenced by site-specific characteristics, such as the geometrical arrangement of electrodes and resistivity variation in the subsurface, both of which have an influence on the magnitude of received voltage. Note also that the total error used to weight each measurement in the inversion should recognize the forward modeling error (often a result of discretization but may include other factors, such as failure to account for three-dimensionality variation in resistivity). In the cases here forward modeling errors were checked, using analytical solutions for uniform flat half-space models, to ensure that forward modeling errors were <1% for all measurements.

2.3. Results and Discussion

[20] ERI was used to image the extent of the alluvial gravel aquifer which exists at varying thicknesses across the floodplain area of the West Brook Farm site. The interpretation of these results was facilitated through the use of geological logs produced from borehole core samples. The sediment sequence has three components: a soil layer at the surface, which is underlain by approximately 4 m of alluvial gravels above the weathered chalk layer. The chalk layer contains regions of more consolidated chalk with flints toward the base of the cores.

[21] The cross-borehole resistivity image from the West Brook Farm site also displays a three layer structure (Figure 3), with an upper conductive layer (4–75 Ωm; $\log_{10}$ resistivity range: 0.55–1.88) interpreted as a thin cover of soil. In the proximity of the boreholes this soil layer is approximately 1 m thick from the resistivity image in both cases, corresponding well with the geological logs. The more conductive values within the soil layer around borehole E are likely due to the presence of peat which was observed in the geological logs of this borehole. The boundary between the lower two resistivity regions correlates well with the interface previously logged between the alluvial gravels (95–1500 Ωm; $\log_{10}$ resistivity range: 1.98–3.18) and underlying weathered chalk (10–75 Ωm; $\log_{10}$ resistivity range: 1.00–1.88). We calculated from the cross borehole resistivity model that the interfaces between the alluvial gravel layer and surrounding layers correlated well with the 95 Ωm contour. Using this value to partition the alluvial gravels we observed that the thickness of this layer varies between 4 and 7 m across the 2-D image, and is confirmed to be continuous beneath the stream channel. The alluvial gravels are underlain by the weathered chalk which displays a lower resistivity. The region of higher resistivity that occurs toward the base of borehole E was correlated with a more consolidated, hence more resistive, section of chalk with flints. It should be noted that there will be a degree of spatial variability in the uncertainty of the location of the interpreted boundaries for these resistivity images. This results from the decrease in resolution with increasing distance from the electrodes.

[22] In this study we were primarily interested in determining the thickness and structure of the alluvial gravels across the floodplain to be used in subsequent work to constrain hydrological modeling. We observed from the cross borehole resistivity image that the alluvial gravel layer varies in thickness beneath the stream channel, a detail that would be missed if interpolating the structure of this layer between the available borehole geological logs. By combining a number of these cross stream ERI transects with traditional surface ERI across the floodplain we could construct a 3-D image of the structure and volume of these alluvial gravels at a site in a relatively short time span. This field study demonstrates the way in which ERI can be used to obtain uninterrupted information about the distribution of the alluvial aquifer across the riparian zone; information that

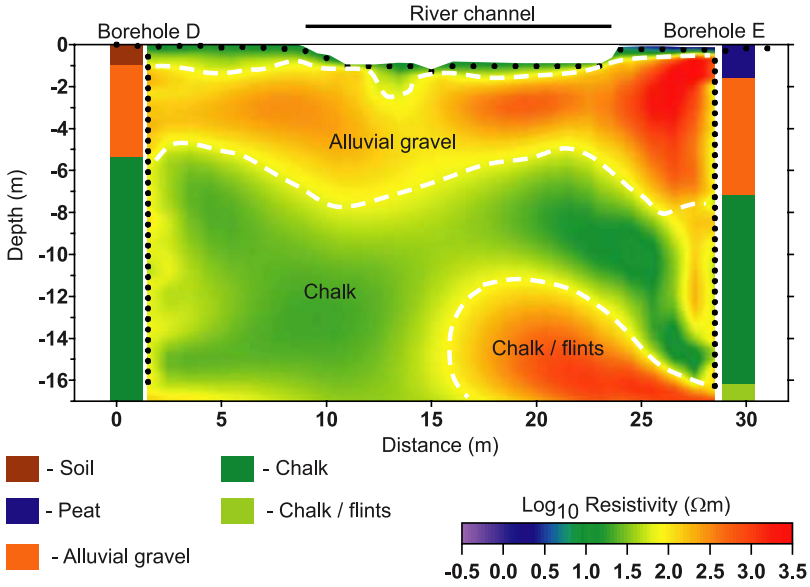

Figure 3. Electrical resistivity model from the cross-borehole survey at the West Brook Farm site. The locations of the surface and borehole electrodes are indicated by the black circles. The geological logs from the core analysis of each borehole are included for comparison, and the key for these can be found at the bottom left of the figure.

is needed in order to develop accurate models of the interactions between groundwater and surface water. Although not addressed here, note also that the study provides a baseline case that may be used in the monitoring of the movement of an electrically contrasting tracer injected into the image plane. Such an in investigation would permit an in situ assessment of the direction and velocity of solutes at the groundwater - surface water interface.

3. Mack Creek, H. J. Andrews Experimental Forest, Oregon, USA

3.1. Site Description and Motivation

[23] Mack Creek is a third-order headwater stream in the H. J. Andrews Experimental Forest, a 6400-ha drainage basin of Lookout Creek within the McKenzie River watershed (Figure 4a). Elevation ranges from 420 m to 1615 m. Our site is an excellent example of a regionally typical, steep, old-growth, conifer-dominated catchment and associated riparian ecosystem. Site bedrock is composed of andesitic lava flows of Miocene age. Catchment evolution is dominated by stream erosion, landslides, debris flows, and past alpine glacial processes, which have resulted in a deeply dissected, steep landscape [*Swanson and James*, 1975; *Swanson and Jones*, 2002].

[24] The site and its environs have been featured in several important stream ecology studies, including the development of the river continuum concept [*Vanotte et al.*, 1980; *Minshall et al.*, 1983] and the quantification of headwater stream nitrogen budgets [*Peterson et al.*, 2001]. Work at Mack Creek and other nearby sites has indicated that the hyporheic zone plays an important role in the overall nitrogen budget of a stream, both as a source [*Wondzell and Swanson*, 1996] and a sink [*Haggerty et al.*, 2005]. Improving our understanding of the hyporheic zone architecture is critical to understanding the overall catchment nutrient dynamics.

[25] The hyporheic zone structure of Mack Creek and many headwater streams around the world is a result of debris dams, produced primarily by large wood or log jams [*Marston*, 1982; *Thompson*, 1995], which have been transported to the valley bottom either by debris flows or direct tree fall. These debris dams can trap stream sediment and organic materials, plus generate sufficient hydraulic gradients required to cycle stream waters into and out of the channel sediments [*Kasahara and Wondzell*, 2003]. To develop realistic models and simulations of hyporheic processes in the sediment behind these debris jams one must know the thickness of trapped sediment with which the hyporheic water exchanges. Obtaining measurements of this thickness proves to be a significant challenge in these periodically high-energy stream environments where the streambed sediments range from sands to boulders as large as several meters in diameter (Figure 5). Drilling and coring is not feasible through these sediments and so the volume of sediment is a critical unknown in modeling efforts. Our geophysics field experiment was designed to determine whether ERI could be used to estimate the distribution and thickness of these heterogeneous sediments behind a debris dam in Mack Creek.

3.2. Methodology

[26] We collected three electrical resistivity lines across a sediment wedge produced by a debris dam in Mack Creek (lines L1, L2, and L3 in Figure 4b). The lines were oriented along the flow direction in the stream channel (i.e., parallel to the valley axis). Positioning of these lines was primarily constrained by the narrow riparian zone and steep adjacent hillslopes, and secondarily by the large boulders and debris in the stream channel (Figures 4b and 5a). Additionally, a calibration survey was conducted downstream where known

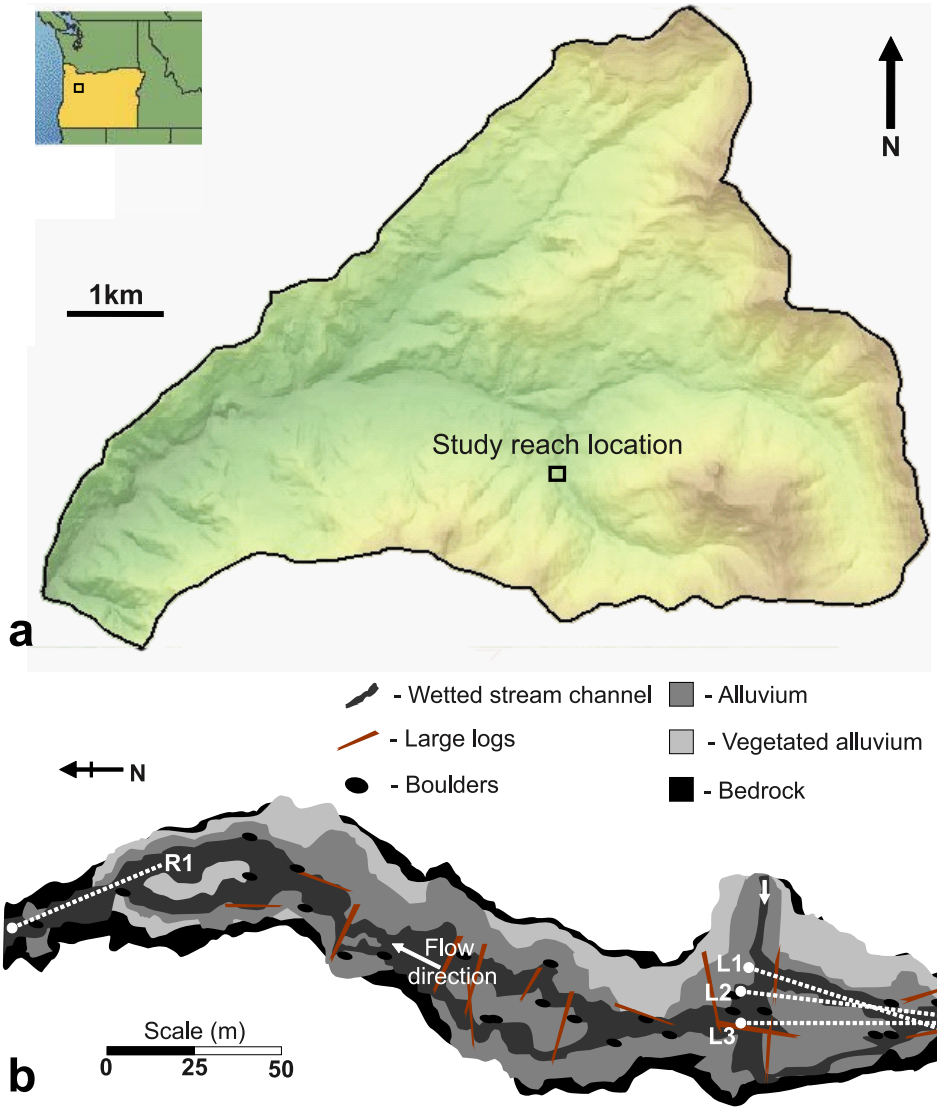

Figure 4. (a) Map showing the location of the H. J. Andrews Research Forest, Oregon, USA, and the study reach of Mack Creek. (b) Plan view schematic of the Mack Creek study reach, outlining the underlying geology and location of the resistivity lines (L1, L2, L3, and R1).

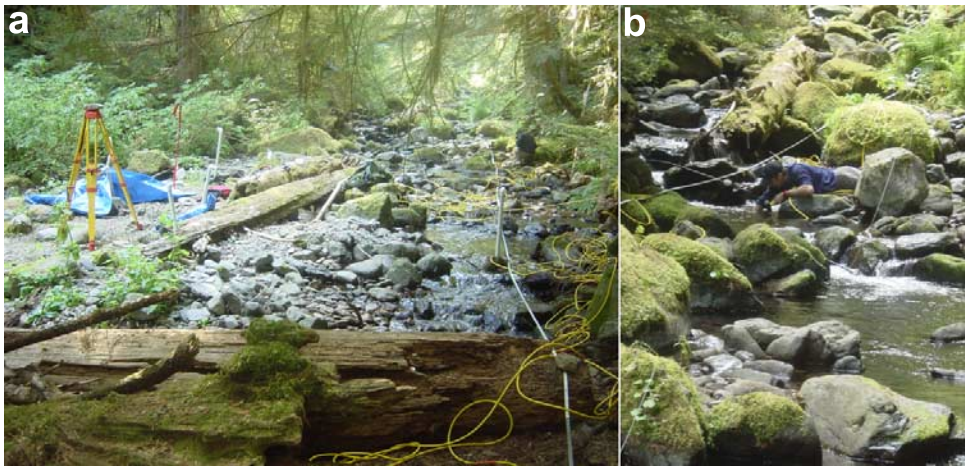

Figure 5. (a) View upstream along electrical resistivity line L3 illustrating the complex terrain consisting of large logs and boulders on the surface of the sediment wedge. (b) View along electrical resistivity line L1 during insta of the electrodes in the streambed sediments below the water column.

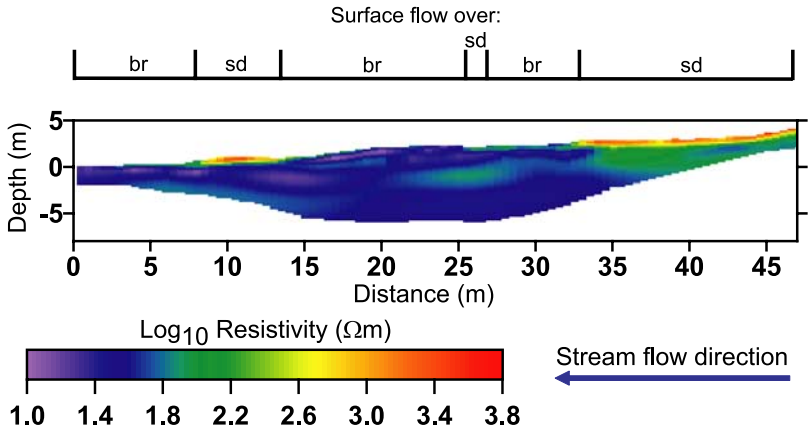

Figure 6. Electrical resistivity model for the Wenner electrode configuration for line R1; a schematic is included of the streambed properties for the resistivity line, indicating the regions where the surface flow is over bedrock (br) or alluvial sediments (sd).

transitions from siliclastic alluvial sediment to bedrock occur (line R1 in Figure 4b). At the main survey area, a section of bedrock outcrop occurred in the streambed immediately upstream from the sediment wedge. Therefore lines L1 and L3 transition from electrodes emplaced in alluvial sediment to bedrock at approximately 44 m along each line. This outcrop was mapped as a weathered andesitic tuff, which is also the same lithology as the exposed bedrock in the downstream calibration reach.

[27] The large proportion of outcropping bedrock along the calibration reach made direct emplacement of traditional stainless steel electrodes time consuming. Therefore the calibration survey was conducted using a submersible borehole electrode array cable; all the electrodes were submerged and placed in direct contact with the bedrock or alluvial sediments for this line. The sections of the calibration line between 0 and 8 m, 13 and 25 m, and 27 and 32 m corresponded to exposed bedrock on the streambed (denoted as "br" in Figure 6). While within the remaining sections of the reach the bedrock was covered by intermittent veneers of sediment (shown as "sd" in Figure 6) that we could manually excavate to locate the interface and alluvial thickness.

[28] Resistance measurements for all lines were collected using a Syscal R1 + Switch48 resistivity system, with 48 electrodes at 1-m intervals. A number of electrode configurations were used to acquire the resistivity data; the pole-pole, dipole-dipole and Wenner configurations were used for lines L1, L2, and L3, while the pole-pole configuration was omitted for line R1 (for details on the various electrode configurations see *Binley and Kemna* [2005]). The pole-pole electrode configuration is presented here for lines L1, L2, and L3, and was chosen to obtain greater depth penetration of the signal with respect to the constrained length of the resistivity lines than the Wenner and dipole-dipole electrode configurations. The remote electrodes were each placed several hundred meters away from the main survey area, in the upstream and downstream directions (>10 times the maximum electrode separation). The Wenner and dipole-dipole configurations were used to provide higher-resolution images of the stream channel sediment structure but to shallower depths, typically <7 m, but are not presented here.

[29] This section of Mack Creek stream channel is predominantly of step-pool morphology, except where the flow shallows and broadens into multiple shallow channels across the surveyed sediment wedge. Given the varying water column height, the layout of the resistivity lines required that a large proportion of the electrode positions needed to be installed in the streambed sediments. When installed, these electrodes were electrically insulated from the water column using a similar procedure employed in the previous River Lambourn study. All electrode locations were surveyed using a total station, and the depth of the water column was measured for those electrodes installed under water for inclusion into the inversion process.

[30] Reciprocal measurements were collected to provide an assessment of errors in the data acquisition process as described previously. Assessment of the reciprocal errors show that on average 90% of the original 750 readings collected for the pole-pole electrode configuration data displayed errors below the 4% cutoff used for this survey.

3.3. Results and Discussion

[31] The electrical resistivity calibration line, collected across known transitions between the bedrock and alluvial sediments, is presented in Figure 6 for the Wenner electrode configuration. The sections of the transect corresponding to the bedrock, between 0 and 8 m, 13 and 25 m, and 27 and 32 m, are characterized by more conductive material. Between 8 and 13 m there is an increase in resistivity in the near surface that corresponds with the silicic boulders and the sediments within a step-pool sequence. A small increase in resistivity is observed in the near surface between 25 and 27 m corresponding to a thin sediment cover on the streambed (typically< 0.2 m in thickness). From 32 m onward, the near surface resistivity values again increase, corresponding to the transition between bedrock and an alluvial sediment bar observed in this region.

[32] The calibration line resistivity model clearly indicates a sharp contrast between the bedrock resistivity and alluvial sediment resistivity signatures. Manual excavations of alluvium at the sediment locations along the calibration

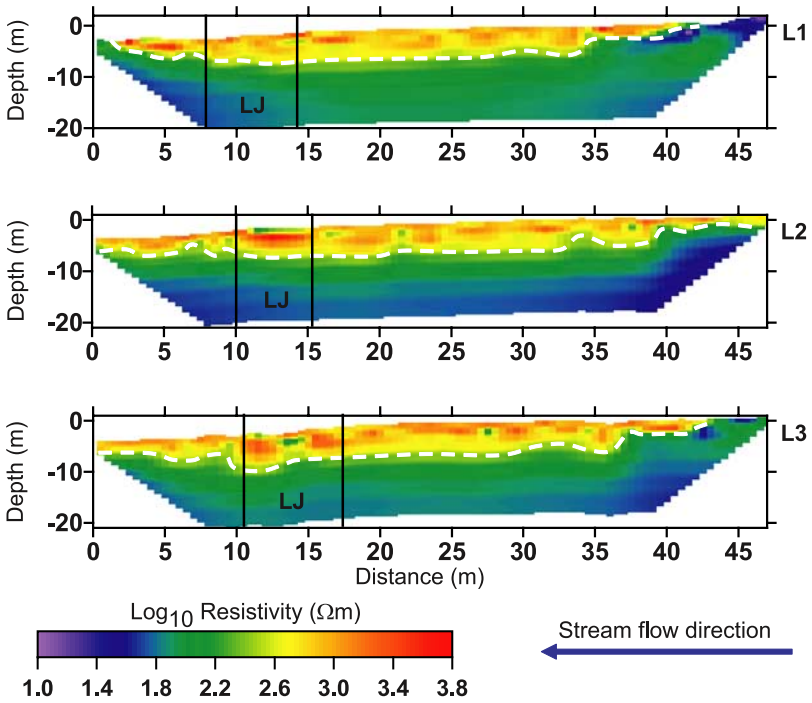

Figure 7. Electrical resistivity models for the pole-pole electrode configuration for lines L1, L2, and L3. The interval between the vertical lines, labeled LJ, indicates the surface location of the fallen logs forming the debris dam. The dashed white line indicates the interpreted bedrock-alluvial sediment boundary.

line found an average alluvial sediment thickness of between 0.75 and 0.90 m, corresponding well to the ERI sediment imaging between 8 and 13 m and 32 m onward. This transition between bedrock and alluvium correlates well with the 200–300 Ωm ($\log_{10}$ resistivity range: 2.30–2.47 Ωm) contour on the electrical resistivity image.

[33] The resistivity models for the pole-pole electrode configuration are shown in Figure 7. The pole-pole data provided here produced a penetration depth of about 18 m, with the 1-m electrode interval, ensuring the interface between bedrock and alluvial sediments would be imaged satisfactorily. The values of resistivity in these models can be compared with the range of resistivity values obtained from the calibration line. The lower limit for the alluvial sediments resistivity was 200–300 Ωm on the basis of analysis of the calibration line. This alluvial resistivity signature provides for a means of delineating between the alluvium and the bedrock. Care must be taken with the use of the above procedure. As with any surface based geophysical technique the resolution of these electrical resistivity models decreases with depth. The interpreted transition between bedrock and alluvial sediments for line L1, L2, and L3 will contain a higher degree of uncertainty owing to the smearing effect of this loss of resolution compared to the calibration line. These limitations are small compared to the errors involved in estimating the thickness of the alluvial sediments from the available traditional hydrogeological information.

[34] Using the 200–300 Ωm lower limit for the alluvial sediments resistivity we can filter out all higher values of resistivity for the 3 lines collected to construct a high-resolution image of the bedrock topography. The location of the debris dam is indicated in Figure 7. This ERI provides a constrained estimate of the thickness of the alluvial sediment package at this site, previously unattainable through other methods. All three images are highly consistent indicating a sediment thickness of approximately 5 m in the region of the debris dam, this increases to as much as 6 m deep just upstream from the debris dam. Moving upstream the sediment wedge eventually tapers off as it approaches the outcropping bedrock exposure at the end of the transects. Records from well installation on the surveyed sediment wedge corroborate these findings as bedrock refusal was not encountered during installations up to 2.5 m below the surface.

[35] Using the delineated resistivity as the bottom boundary of the sediment package a first-order estimate of the sediment package volume can be made using the 3 lines. By assuming a linear interpolation between each line along the interpreted boundary of the sediment package and between the same boundary along the outer two lines and the respective lateral valley bottom walls provides an estimate of 5400 m^3 of sediment being held behind the debris dam. This first approximation of the sediment volume and detailed sediment geometry can now be used to inform hydrogeologic models of the stream dynamics, such as the hyporheic exchange through this sediment wedge.

4. Conclusions

[36] A desire to improve the understanding of hydrological processes often requires that measurements be made in challenging environments where traditional techniques prove unfeasible or inadequate. We have demonstrated that

ERI, with the recent advancements in acquisition and inversion methods, coupled with a few simple ERI tool modifications provides an indispensable method for determining sediment characteristics underlying stream channels. By emplacing the electrodes directly in the sediments of the streambed we demonstrate that high-resolution images of subsurface sediment architecture, directly beneath the water column, can be obtained. This technique provides a seamless image across the transition between riparian zone and stream channel at the lowland Lambourn River site and the longitudinal alluvium-bedrock contact at the headwater Mack Creek sites. Both ERI site findings represent significant advances in our understanding about the subsurface, its architecture and connectivity than the information normally attainable from boreholes alone.

[37] In both of the examples, ground-truthing the electrical resistivity models through comparison with alternative forms of subsurface information isolated the resistivity values for the lithologies of interest. These calibrations were then applied to all regions of the resistivity lines, allowing the interpretation of the architecture for each site to be determined beneath the stream channel. Hence, the uninterrupted location and geometry of the alluvial gravel aquifer across the floodplain at the River Lambourn site and the depth and volume of the trapped alluvial sediments behind the debris dam of Mack Creek can be determined. This information can be used to inform subsequent hydrological investigations and models of these stream systems. In particular the example from Mack Creek, in the H. J. Andrews Research Forest, illustrates the flexible nature of this ERI technique when designing the data acquisition in challenging terrain, where otherwise it is very difficult to obtain subsurface information.

[38] **Acknowledgments.** This material is based on work supported by the U.S. National Science Foundation (NSF) under grants 03-26064, 04-47287, and EAR 04-09534 and by the UK Natural Environment Research Council (NERC) LOCAR program under grant NER/T/S/2001/00948. Any opinions, findings, and conclusions or recommendations expressed in this material are those of the authors(s) and do not necessarily reflect the views of the NSF or NERC. The use of firm, trade, and brand names in this report is for identification purposes only and does not constitute endorsement by CUAHSI, NSF, NERC, the U.S. government, or the authors and their respective institutions.

References

Acworth, R. I., and G. R. Dasey (2003), Mapping of the hyporheic zone around a tidal creek using a combination of borehole logging, borehole electrical tomography and cross-creek electrical imaging, New South Wales, Australia, *Hydrogeol. J.*, *11*, 359–372, doi:10.1007/s10040-003-0278-0.

al Hagrey, S. A., and J. Michaelsen (1999), Resistivity and percolation study of preferential flow in vadose zone at Bokhorst, Germany, *Geophysics*, *64*(3), 746–753, doi:10.1190/1.1444584.

Andersen, M. S., L. Baron, J. Gudbjerg, J. Gregersen, D. Chapellier, R. Jakobsen, and D. Postma (2007), Discharge of nitrate-containing groundwater into a coastal marine environment, *J. Hydrol.*, *336*, 98–114, doi:10.1016/j.jhydrol.2006.12.023.

Binley, A., and A. Kemna (2005), DC resistivity and induced polarization methods, in *Hydrogeophysics*, edited by Y. Rubin and S. S. Hubbard, pp. 129–156, Springer, New York.

Binley, A., A. Ramirez, and W. Daily (1995), Regularized image reconstruction of noisy electrical resistance tomography, in *Process Tomography '95: Implementation for Industrial Processes*, edited by M. S. Beck et al., pp. 401–410, Univ. of Manchester Inst. of Sci. and Technol., Manchester, U. K.

Binley, A., P. Winship, L. J. West, M. Pokar, and R. Middleton (2002), Seasonal variation of moisture content in unsaturated sandstone inferred from borehole radar and resistivity profiles, *J. Hydrol.*, *267*, 160–172, doi:10.1016/S0022-1694(02)00147-6.

Bradford, R. B. (2002), Controls on the discharge of chalk streams of the Berkshire Downs, UK, *Sci. Total Environ.*, *282/283*, 65–80, doi:10.1016/S0048-9697(01)00954-8.

Breier, J. A., C. F. Brier, and H. N. Edmonds (2005), Detecting submarine groundwater discharge with synoptic surveys of sediment resistivity, radium, and salinity, *Geophys. Res. Lett.*, *32*, L23612, doi:10.1029/2005GL024639.

Burkholder, B. K., G. E. Grant, R. Haggerty, T. Khangaonkar, and P. J. Wampler (2008), Influence of hyporheic flow and geomorphology on temperature of a large, gravel-bed river, Clackamas River, Oregon, USA, *Hydrol. Processes*, *22*, 941–953, doi:10.1002/hyp.6984.

Constable, S. C., R. L. Parker, and C. G. Constable (1987), Occam's inversion: A practical algorithm for generating smooth models from electromagnetic sounding data, *Geophysics*, *52*(3), 289–300, doi:10.1190/1.1442303.

Daily, W., A. Ramirez, D. LaBrecque, and J. Nitao (1992), Electrical resistivity tomography of vadose water movement, *Water Resour. Res.*, *28*, 1429–1442, doi:10.1029/91WR03087.

Day-Lewis, F. D., E. A. White, C. D. Johnson, J. W. Lane, Jr., and M. Belaval (2006), Continuous resistivity profiling to delineate submarine groundwater discharge—Examples and limitations, *Leading Edge*, *25*(6), 724–728, doi:10.1190/1.2210056.

Grapes, T. R., C. Bradley, and G. E. Petts (2005), Dynamics of river-aquifer interactions along a chalk stream: The River Lambourn, UK, *Hydrol. Processes*, *19*, 2035–2053, doi:10.1002/hyp.5665.

Grapes, T. R., C. Bradley, and G. E. Petts (2006), Hydrodynamics of floodplain wetlands in a chalk catchment: The River Lambourn, UK, *J. Hydrol.*, *320*, 324–341, doi:10.1016/j.jhydrol.2005.07.028.

Haggerty, R., J. LaNier, C. L. Crenshaw, S. M. Wondzell, M. Baker, and M. N. Gooseff (2005), Discriminating among transport, reaction-rate, and substrate limitation for hyporheic nitrate retention using $^{15}NO_3^-$ additions: Preliminary results from Mack Creek, Oregon, *Eos Trans. AGU*, *86*, Spring Meet. Suppl.

Jones, J. B., and P. J. Mulholland (Eds.) (1999), *Streams and Ground Waters*, Elsevier, New York.

Kasahara, T., and S. M. Wondzell (2003), Geomorphic controls on hyporheic exchange flow in mountain streams, *Water Resour. Res.*, *39*(1), 1005, doi:10.1029/2002WR001386.

Kemna, A., J. Vanderborght, B. Kulessa, and H. Vereecken (2002), Imaging and characterization of subsurface solute transport using electrical resistivity tomography (ERT) and equivalent transport models, *J. Hydrol.*, *267*, 125–146, doi:10.1016/S0022-1694(02)00145-2.

Kemna, A., A. Binley, and L. Slater (2004), Cross-borehole IP imaging for engineering and environmental applications, *Geophysics*, *69*(1), 97–105, doi:10.1190/1.1649379.

Kwon, H., J. Kim, H. Ahn, J. Yoon, K. Kim, C. Jung, S. Lee, and T. Uchida (2005), Delineation of a fault zone beneath a riverbed by an electrical resistivity survey using a floating streamer cable, *Explor. Geophys.*, *36*, 50–58, doi:10.1071/EG05050.

Manheim, F. T., D. E. Krantz, and J. F. Bratton (2004), Studying ground water under Delmarva coastal bays using electrical resistivity, *Ground Water*, *42*(7), 1052–1068, doi:10.1111/j.1745-6584.2004.tb02643.x.

Marston, R. A. (1982), The geomorphic significance of log steps in forest streams, *Ann. Assoc. Am. Geogr.*, *72*, 99–108, doi:10.1111/j.1467-8306.1982.tb01386.x.

Minshall, G. W., R. C. Petersen, K. W. Cummins, T. L. Bott, J. R. Sedell, C. E. Cushing, and R. L. Vannote (1983), Interbiome comparison of stream ecosystem dynamics, *Ecol. Monogr.*, *53*(1), 1–25, doi:10.2307/1942585.

Peterson, B. J., et al. (2001), Control of nitrogen export from watersheds by headwater streams, *Science*, *292*, 86–90, doi:10.1126/science.1056874.

Singha, K., and S. M. Gorelick (2005), Saline tracer visualized with three-dimensional electrical resistivity tomography: Field-scale spatial moment analysis, *Water Resour. Res.*, *41*, W05023, doi:10.1029/2004WR003460.

Singha, K., F. D. Day-Lewis, and J. W. Lane, Jr. (2007), Geoelectrical evidence of bicontinuum transport in groundwater, *Geophys. Res. Lett.*, *34*, L12401, doi:10.1029/2007GL030019.

Slater, L., and A. Binley (2006), Synthetic and field based electrical imaging of a zerovalent iron barrier: Implications for monitoring long-term barrier performance, *Geophysics*, *71*(5), B129–B137, doi:10.1190/1.2235931.

Slater, L., A. Binley, and D. Brown (1997), Electrical imaging of the response of fractures to ground water salinity change, *Ground Water*, *35*(3), 436–442, doi:10.1111/j.1745-6584.1997.tb00103.x.

Sophocleous, M. (2002), Interactions between groundwater and surface water: The state of the science, *Hydrogeol. J.*, *10*, 52–67, doi:10.1007/s10040-001-0170-8.

Swanson, F. J., and M. E. James (1975), Geology and geomorphology of the H. J. Andrews Experimental Forest, western Cascades, Oregon, 14 pp., U.S. Dep. of Agric. For. Serv., Portland, Oreg.

Swanson, F. J., and J. A. Jones (2002), Geomorphology and hydrology of the H. J. Andrews Experimental Forest, Blue River, Oregon, in *Field Guide to Geologic Processes in Cascadia: Field Trips to Accompany the 98th Annual Meeting of the Cordilleran Section of the Geological Society of America*, edited by G. Moore, pp. 289–314, Oreg. Dep. of Geol. and Miner. Ind., Corvallis, Oreg.

Thompson, D. M. (1995), The effects of large organic debris on sediment processes and stream morphology in Vermont, *Geomorphology*, *11*, 235–244, doi:10.1016/0169-555X(94)00064-X.

Vanotte, R. L., G. W. Minshall, K. W. Cummins, J. R. Sedell, and C. E. Cushing (1980), The river continuum concept, *Can. J. Fish. Aquat. Sci.*, *37*, 130–137.

Wondzell, S. M. (2006), Effect of morphology and discharge on hyporheic exchange flows in two small streams in the Cascade Mountains of Oregon, USA, *Hydrol. Processes*, *20*, 267–287, doi:10.1002/hyp.5902.

Wondzell, S. M., and F. J. Swanson (1996), Seasonal and storm dynamics of the hyporheic zone of a 4th-order mountain stream. II: Nitrogen cycling, *J. N. Am. Benthol. Soc.*, *15*(1), 20–34, doi:10.2307/1467430.

A. Binley, Lancaster Environment Centre, Lancaster University, Lancaster LA1 4YQ, UK.

N. Crook and R. Knight, Department of Geophysics, Stanford University, 397 Panama Mall, Stanford, CA 94305, USA. (ncrook@stanford.edu)

R. Haggerty and J. Zarnetske, Department of Geosciences, Oregon State University, Corvallis, OR 97331, USA.

D. A. Robinson, Department of Food Production, University of West Indies, St. Augustine, Trinidad and Tobago.